JOURNAL OF Materials CHEMISTRY

Synthesis and characterization of the hydrated rare-earth acid diphosphates $LnHP_2O_7{\cdot}3.5H_2O$ (Ln = rare-earth elements)†

S. Ben Moussa,[a] I. Sobrados,[a] J. E. Iglesias,[a] M. Trabelsi-Ayedi[b] and J. Sanz*[a]

[a]*Instituto Ciencia de Materiales, CSIC, Cantoblanco 28049 Madrid, Spain. E-mail: samibm@icmm.csic.es*
[b]*Institut Supérieur de l'Éducation et de la Formation Continue le Bardo, Tunisia*

Received 19th January 2000, Accepted 22nd May 2000
Published on the Web 13th July 2000

Hydrated lanthanum acid diphosphates, of the formula $LnHP_2O_7{\cdot}3.5H_2O$, have been prepared from acidic $LaCl_3$ and $Na_4P_2O_7$ solutions (pH = 1), and characterized by XRD, IR and NMR spectroscopic techniques. In the series Ln = La–Sm, these phosphates crystallize in the orthorhombic system (Type I) but in the series Sm–Yb, they crystallize in the triclinic system (Type II). In the case of Sm diphosphates both structures can be obtained depending on the synthesis conditions. The diphosphate character of the compounds was assessed by IR and NMR and two environments, namely PO_4^{3-} and HPO_4^{2-}, were identified by ^{31}P MAS spectroscopy. Finally, a different distribution of OH and water was deduced from NMR and IR spectroscopic analysis of the two series of diphosphates.

Introduction

The optical properties of rare-earth phosphates have been extensively analyzed because of their possible application as laser materials and phosphors.[1–7] In particular, poly- and ultraphosphates (LnP_5O_{14}) of rare-earth elements have been studied for high power laser applications.[8,9]

Mono-, tetra-, cyclo- and polyphosphates can be prepared from acid diphosphates depending on the temperature and time of treatment.[10] However, decomposition of acid lanthanum diphosphates has not been well documented. Syntheses of acid diphosphates of trivalent cations, $LnHP_2O_7{\cdot}3.5H_2O$, have been reported by several authors. $LaHP_2O_7{\cdot}3.5H_2O$ was first described by Tananaev *et al.*[11] during an investigation of the $La_4(P_2O_5)$–$H_4P_2O_7$–H_2O system. Kizilyalli[10] described the chemical preparation of $HGdP_2O_7{\cdot}nH_2O$ (n = 3–4), and investigated the thermal decomposition of this compound. Afonin and Pechurova[12] prepared $RE^{III}HP_2O_7{\cdot}3.5H_2O$, where RE^{III} = La, Ce, Nd, Eu, Er, Yb, and Y, and identified anhydrous phases of these compounds. However, neither the XRD indexing nor crystalline structure of these compounds have been reported.

In this work, the compounds $HLnP_2O_7{\cdot}3.5H_2O$, where Ln = La, Ce, Pr, Nd, Sm, Eu, Gd, Tb, Dy, Ho, Er and Yb, have been prepared and characterized by XRD (X-ray diffraction), IR (infrared) and NMR (nuclear magnetic resonance) spectroscopic techniques. From the XRD data, the symmetry and unit cell constants have been determined, and from IR and NMR spectra, the structural environments of the P atoms have been analyzed. Depending on the nature of the rare-earth element, two different structures have been identified for the La–Sm and Sm–Yb series.

Experimental section

Materials

The $LnHP_2O_7{\cdot}3.5H_2O$ compounds were prepared by mixing a sodium diphosphate solution ($Na_4P_2O_7$, 0.1 M) and an acidic solution (pH = 1) of the rare earth chloride ($LnCl_3$, 0.1 M), and stirring the resulting solution for two hours at room temperature. The polycrystalline precipitate was filtered off, washed and dried at room temperature. For chemical analysis purposes, the obtained product was dissolved in water (pH = 1) at 150 °C and phosphorus, rare-earth and sodium contents determined by the inductively coupled plasma (ICP) technique. In the case of the Sm diphosphate, two different phases were obtained depending on the relative concentrations of reagents used. The first polymorph was obtained using $SmCl_3$ and $Na_4P_2O_7$ in a molar ratio of 1 : 1; and the second using a ratio of 0.4 : 1.

In the case of La and Er diphosphates, the preparation of single crystals was attempted at different temperatures and compositions. The temperature was varied between 5 and 40 °C, and the molar $Ln:P_2O_7$ ratio was varied between 0.2 and 1.4. In no case was the result satisfactory. To prevent rapid precipitation, a small amount of methanol was added to the solution of diphosphate and lanthanide chloride, while the solution was cooled in a refrigerator at 5 °C. Unfortunately, highly defective ultra-thin platelets were obtained with inadequate characteristics for structural analysis.

Experimental

DTA and TG curves were obtained in a nitrogen atmosphere, with a Stanton Redcroft-780 series instrument, using Pt–Pt 13% Rh thermocouples. The heating rate was 10 °C min^{-1} and an α-Al_2O_3 sample calcined at 1400 °C was used as a reference material. Samples were loosely packed in Pt crucibles. Weight losses produced between room temperature and 1200 °C were calculated as percentages from the TG curves.

XRD powder data were collected on a Philips X'pert diffractometer fitted with an incident beam Ge(111) curved crystal monochromator, under strictly monochromatic conditions [λ(Cu-Kα_1) = 1.5405981 Å]. Data were taken between $8° \leqslant 2\theta \leqslant 70°$ with a step width of 0.02°, and equatorial divergence of 0.5°. The receiving slit was 0.05 mm (0.012°, R = 230 mm) and Soller slits of 1° were inserted in front of the counter. The sample was spun at 2 Hz around an axis normal to the sample surface and counts were measured for 6 s at each step. Peak positions were determined with the help of the diffractometer software, but, in the case of serious overlap, they were measured by hand. A small amount of Si (NIST, a = 5.430940 Å) was mixed with the sample in a second run

†Full details of the indexing of the X-ray powder pattern of the La and Yb compounds are available as Tables 1 and 2 in electronic supplementary information (ESI). For direct electronic access see http://www.rsc.org/suppdata/jm/b0/b000543f/

to determine precisely the correction ($<0.01^\circ$) to be applied to the observed peak positions.

The samples were diluted with KBr to form pellets (phosphate/KBr = 5% by weight) and examined by IR spectrometry in the 240 to 4000 cm^{-1} region, using a Nicolet 20 SXC FT-IR spectrometer. A high purity polystyrene foil was used to calibrate the spectrophotometer; errors in the band positions were estimated as less than 2 cm^{-1}.

^{31}P NMR spectra were recorded at 161.96 MHz using an MSL-400 Bruker spectrometer. The samples were spun at 4 kHz. MAS spectra were taken after a $\pi/2$ pulse irradiation (6 μs). The number of scans was 20 and the time interval between successive scans 5 s. CP-MAS spectra were obtained using the standard cross-polarization pulse technique. The Hartman–Hann condition was obtained with a radiofrequency H_1 field of 15 G for the decoupler channel (400.13 MHz). For the recorded spectrum, a contact time of 1 ms and a period between successive accumulations of 5 s were chosen. The number of scans was 40. In both techniques the filter band width used was 60 kHz. Chemical shifts are reported in parts per million (ppm) from an external 85% H_3PO_4 aqueous solution.

Analysis of the MAS and CP-MAS spectra was carried out by using the Bruker program WINFIT.[13] The spinning rate and the positions, linewidths and intensities of the components were determined with a standard, non-linear least squares fitting method. Chemical shift anisotropies ($\Delta\sigma$ and η) of NMR components are adaptable parameters that must be determined by trial and error. For quantitative purposes, the sum of integrated intensities of all side bands corresponding to each component was determined.

Results

Chemical and thermal analysis

The elemental compositions of the two end-member diphosphates were determined. Na, P, Ln compositions were determined by ICP (inductively coupled plasma) and Cl contents by ISE (ion selective electrode) techniques, as described above in the experimental section. Chemical analysis data obtained on dehydrated samples are in good agreement with those calculated for the structural formula $LnHP_2O_7$. Analysis found for $LaHP_2O_7$: P, 16.3; La, 36.6; and for $YbHP_2O_7$: P, 15.0; Yb, 41.9%. In all cases the amount of Na and Cl measured was very low (Cl/P, Na/P <0.005).

From thermal analysis, the total weight loss determined in the range 20–900 °C, corresponds to 3.5 molecules of water per formula unit (Fig. 1) for all compounds. In most cases, water of crystallization is lost in two stages, the first two molecules are lost near 100 °C and those remaining at around 200 °C. The OH elimination begins at 200 °C and is complete at 600 °C in the La–Sm (I) series and 900 °C in the Sm–Yb series. The DTA curves exhibit endothermic bands associated with the loss of H_2O and OH groups (Fig. 1). Narrow peaks detected below 200 °C are due to water elimination, and broad peaks detected between 200 and 900 °C are due to OH elimination. Exothermic peaks detected above 700 °C have been assigned to decomposition of diphosphates and formation of new phases.

X-Ray study

The XRD patterns of $LnHP_2O_7{\cdot}3.5H_2O$ diphosphates display narrow peaks, characteristic of well-crystallized compounds (Fig. 2). However, the number of peaks in the La–Sm series is lower than in the Sm–Yb series, indicating different symmetry in both types of compounds.

In the case of $LaHP_2O_7{\cdot}3.5H_2O$, the first 25 reflections were indexed automatically[14] after correction of the three lowest angle Bragg peaks with values obtained from their higher orders (3rd, 2nd and 3rd, respectively). An orthorhombic symmetry was found for which the quality estimators were judged sufficiently good ($M_{20}{}^{15}=41$ and $F_{20}{}^{16}=89$). The lattice parameters were then refined using 84 observed lines up to $2\theta=70^\circ$ (see Table 1, electronic supplementary information†). All lines were indexed, confirming the single phase character of the sample. After refinement with Hess weights, the final parameters obtained for this compound were: $a=18.489(1)$, $b=13.6132(8)$, $c=6.8570(5)$ Å and $V=1725.9$ $Å^3$, with $|2\theta_{obs}-2\theta_{calc}|\leqslant 0.025^\circ$ for all observations. The final reliability estimators for this indexing were: $M_{20}=69$, ($\langle\varepsilon\rangle=0.000020$), $F_{20}=148$ (0.005881, 23); $M_{30}=59$, ($\langle\varepsilon\rangle=0.000022$), $F_{30}=135$ (0.005719, 39); $M_{84}=16$, ($\langle\varepsilon\rangle=0.000048$), $F_{84}=52$ (0.007837, 207). From the indexed lines, systematic absences were noted: hkl, $h+l=2n$; $0kl$, $k=2n$; $h0l$, $h=2n$ ($l=2n$). From the systematic absences, the possible space group could be either *Bba*2 (no. 41) or *Bbcm* (no. 64) [standard setting, *Cmca*]. This structure is hereafter referred to as type I. We carried out an independent indexing process with a different algorithm, as implemented in the DICVOL91 program,[17] using the first 20 observed reflections. The result was the same orthorhombic solution as given above, with $M_{20}=38$, $F_{20}=79$, plus two more monoclinic primitive solutions which turned out to be redundant.

In the case of $YbHP_2O_7{\cdot}3.5H_2O$, the first 39 reflections were used in the starting indexing. A triclinic solution was found with TREOR[14] for which the quality estimators were judged good ($M_{20}=70$ and $F_{20}=130$). The lattice parameters were refined using 70 observed lines up to $2\theta=44^\circ$ (see Table 1, electronic supplementary information†). All lines were indexed, confirming the absence of secondary phases. The final parameters obtained for this compound were: $a=6.3767(3)$, $b=6.8159(3)$, $c=9.7833(4)$ Å, $\alpha=81.699(4)$, $\beta=80.009(4)$, $\gamma=88.311(5)^\circ$ and $V=414.4$ $Å^3$, with $|2\theta_{obs}-2\theta_{calc}|\leqslant 0.01^\circ$. The final reliability estimators for this compound were: $M_{20}=87$, ($\langle\varepsilon\rangle=0.000014$), $F_{20}=171$ (0.00510, 23); with $M_{30}=61$, ($\langle\varepsilon\rangle=0.000016$), $F_{30}=161$ (0.00503, 37); $M_{70}=33$, ($\langle\varepsilon\rangle=0.000021$), $F_{70}=145$ (0.00470, 103). The space group is either $P1$ or $P\bar{1}$. This structure type is referred to as type II in what follows. As in the orthorhombic case above, an independent indexing was attempted with DICVOL91,[17] using the first 20 observed reflections. No solution was found for symmetry higher than triclinic. Two triclinic solutions were found, with $M_{20}=88$ and 84. The first was identical with that found by TREOR (which was the Niggli-reduced cell) and the second was a different primitive of the same lattice ($\vec{a}'=\vec{a}-\vec{c}$, $\vec{b}'=b$, $\vec{c}'=-\vec{a}$).

The XRD patterns of the other diphosphates were indexed by analogy with those of La and Yb diphosphates. Results are displayed in Table 1, where unit cell contractions are observed in the two series of compounds as a function of the rare-earth radii. In the case of Sm diphosphates, the unit cell parameters of the two crystalline phases are included.

IR study

The IR spectra of the diphosphates described are shown in Fig. 3. Bands in the region 3700–3100 cm^{-1} and 1700–1600 cm^{-1} can be attributed to OH/H_2O vibrations and bands below 1300 cm^{-1} to diphosphate modes. The analysis of H_2O bending mode bands (1630–1650 cm^{-1}) confirmed the existence of two types of water. In the case of diphosphates of type II, the stretching modes of water molecules are more intense and located at lower frequencies, suggesting the existence of stronger hydrogen bonds for water. In all cases, the band at 3200 cm^{-1}, which remained after dehydratation (not shown in the figure), was assigned to POH stretching modes.

In the 400–1300 cm^{-1} region of the IR spectra of the La–Sm series, two maxima at 1100–1200 and 1050–1100 cm^{-1} are

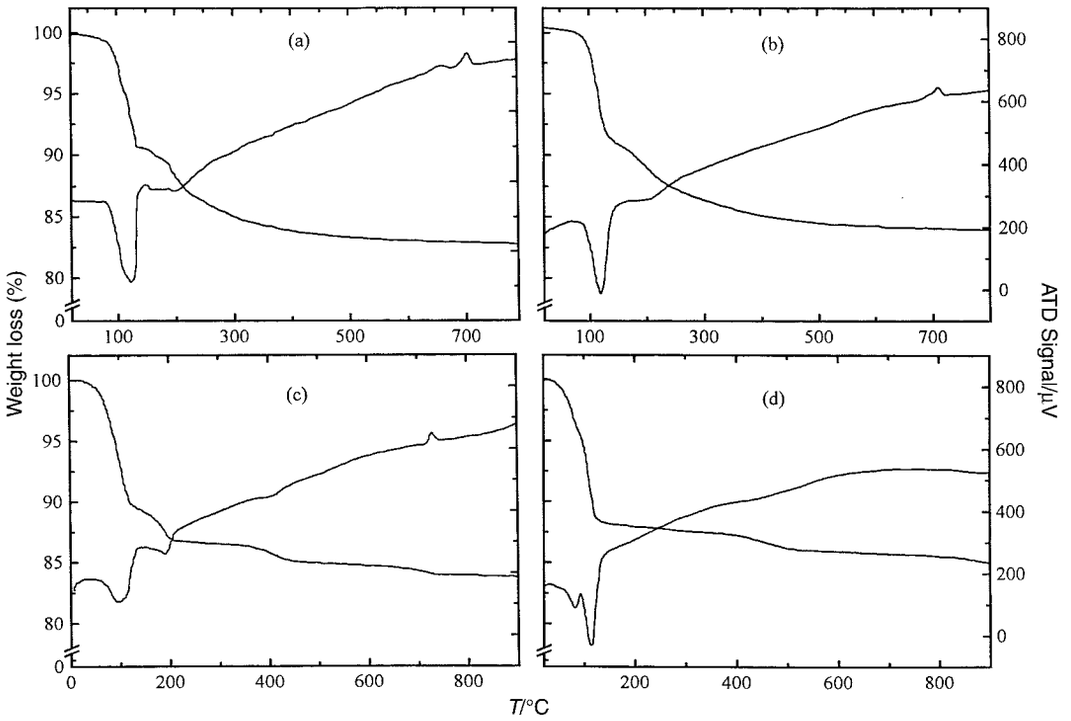

Fig. 1 DTA and TG curves of $LaHP_2O_7{\cdot}3.5H_2O$ (a), $SmHP_2O_7{\cdot}3.5H_2O$ (type I) (b), $SmHP_2O_7{\cdot}3.5H_2O$ (type II) (c), and $YbHP_2O_7{\cdot}3.5H_2O$ (d).

detected that are ascribed to antisymmetric $\nu_{as}(PO_3)$ and symmetric $\nu_s(PO_3)$ vibrations of the P tetrahedra. Bands around 950 and 750 cm^{-1} were ascribed to the antisymmetric and symmetric vibration of POP groups, confirming the diphosphate character of these compounds.[18] Finally, the complex band located at 500 cm^{-1} corresponds to vibration modes of diphosphate and the octahedrally coordinated lanthanum. In the IR spectra of the the Sm–Yb series, the number of intense modes in the range 800–1300 cm^{-1} is higher than that in the La–Sm series. In particular, each mean band of diphosphate is split into at least two components, indicating that the symmetry of the first compounds must be lower.

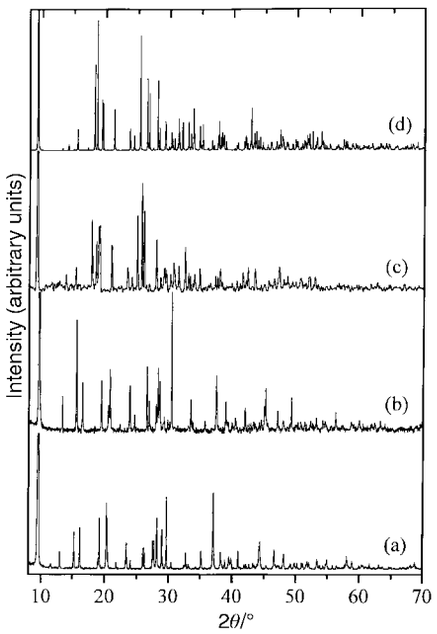

Fig. 2 X-Ray powder diffraction patterns of $LaHP_2O_7{\cdot}3.5H_2O$ (a), $SmHP_2O_7{\cdot}3.5H_2O$ (type I) (b), $SmHP_2O_7{\cdot}3.5H_2O$ (type II) (c), and $YbHP_2O_7{\cdot}3.5H_2O$ (d) recorded at room temperature under monochromatic conditions [λ(Cu-Kα_1) = 1.5405981 Å].

However, the assignment of bands to the different possible modes is not easy.

NMR study

^{31}P MAS-NMR spectra of the La, Sm (type I) and Sm (type II) diphosphates recorded after a $\pi/2$ pulse irradiation, are shown in Fig. 4(a). The analysis of the NMR spectra of the other diphosphates was difficult due to the paramagnetic interactions between P and Ln atoms that broaden the NMR lines.

In the phosphates analyzed, MAS-NMR spectra are formed by two components and their corresponding spinning side bands spaced at 25 ppm (spinning rate expressed in cps). In the spectra of the Sm diphosphate of type I, the bands are wider, making resolution into two components difficult (see Fig. 4 inset). In the spectra of the other two diphosphates, components at higher chemical shift values are broader than those at lower values. In order to reduce residual H–P dipolar interactions, CP-MAS spectra were recorded. In these spectra, the linewidths of the first components were reduced; however, resolution into two components in $SmHP_2O_7{\cdot}3.5H_2O$ (type I) was still not possible. Isotropic chemical shift values δ_{iso} of the components are given in Fig. 4.

From the ^{31}P MAS-NMR spectra, integrated intensities of the two central components have been estimated, as well as the intensities of the side bands of each component. In the MAS spectra of these samples, the intensities of both components are similar. However, the intensities in CP-MAS spectra differ from those obtained in MAS spectra. In particular, in the two samples of type I phosphates, $LaHP_2O_7{\cdot}3.5H_2O$ and $SmHP_2O_7{\cdot}3.5H_2O$ (type I), the integrated intensities of both components are similar; however, in the case of the type II phosphate, $SmHP_2O_7{\cdot}3.5H_2O$ (type II), the intensity of the peak at −11.8 ppm is higher than that of the resonance at −18.3 ppm. Observed differences in the intensities of these two components in the MAS and CP-MAS spectra suggest the existence of different hydrogen bond configurations in the two types of phosphates. A discussion of this point can be found below.

In all cases the MAS-NMR patterns are very broad (150, −150 ppm) indicating that chemical shift anisotropies are more

Table 1 Unit cell parameters of the compounds analyzed. The M_{20} agreement factors are given in the last column

Compound	a/Å	b/Å	c/Å	α/°	β/°	γ/°	V/Å^3	M_{20}
$LaHP_2O_7{\cdot}3.5H_2O$ (I)	18.489(1)	13.6132(8)	6.8570(5)				1725.9	69
$CeHP_2O_7{\cdot}3.5H_2O$ (I)	18.4636(4)	13.5177(4)	6.8205(2)				1702.3	50
$PrHP_2O_7{\cdot}3.5H_2O$ (I)	18.4403(8)	13.4553(4)	6.7943(1)				1685.8	35
$NdHP_2O_7{\cdot}3.5H_2O$ (I)	18.3914(7)	13.3839(4)	6.7629(2)				1664.7	55
$SmHP_2O_7{\cdot}3.5H_2O$ (I)	18.3260(6)	13.2763(4)	6.7195(3)				1634.9	35
$SmHP_2O_7{\cdot}3.5H_2O$ (II)	6.4985(2)	7.0344(3)	9.8192(5)	81.463(4)	80.665(4)	88.292(4)	438.0	65
$EuHP_2O_7{\cdot}3.5H_2O$ (II)	6.4798(3)	6.9971(3)	9.8059(5)	81.487(5)	80.610(5)	88.324(5)	433.8	58
$GdHP_2O_7{\cdot}3.5H_2O$ (II)	6.4641(2)	6.9787(3)	9.8070(3)	81.520(4)	80.557(3)	88.377(3)	431.6	65
$TbHP_2O_7{\cdot}3.5H_2O$ (II)	6.4498(4)	6.9465(4)	9.8129(5)	81.647(7)	80.377(6)	88.356(5)	428.9	82
$DyHP_2O_7{\cdot}3.5H_2O$ (II)	6.4306(3)	6.9066(3)	9.7935(5)	81.618(5)	80.384(4)	88.413(4)	424.3	78
$HoHP_2O_7{\cdot}3.5H_2O$ (II)	6.4140(2)	6.8922(2)	9.7980(3)	81.669(3)	80.273(3)	88.407(3)	422.4	106
$ErHP_2O_7{\cdot}3.5H_2O$ (II)	6.4048(2)	6.8697(2)	9.7954(3)	81.658(4)	80.186(3)	88.477(4)	420.2	79
$YbHP_2O_7{\cdot}3.5H_2O$ (II)	6.3767(3)	6.8159(3)	9.7833(4)	81.699(4)	80.009(4)	88.311(5)	414.4	87

important than P–P or P–H dipolar interactions. From the analysis of the sideband patterns, the anisotropies of the chemical shift tensors were estimated; in all cases, the anisotropies $\Delta\sigma$ are near 90 ppm, however the sign is different in the two families of diphosphates. Asymmetry values are always near 0.8, indicating a clear departure from axial symmetry for the P environments, in agreement with the orthorhombic or triclinic symmetries of these phosphates.

Discussion

Chemical analysis carried out on dried rare-earth diphosphates confirmed that compounds $LnHP_2O_7{\cdot}3.5H_2O$ were formed according to the following reaction:

$$4Na_4P_2O_7 + 4LnCl_3{\cdot}6H_2O + 4HCl \rightarrow 4LnHP_2O_7{\cdot}3.5H_2O + 16NaCl + 10H_2O$$

In all phosphates, the relative amounts of P and La conform to a molar ratio Ln : P ≈ 1 : 2 and the amounts of Na and Cl remaining are negligible.

All diphosphates display similar DTA/TG curves, in which water and OH losses are differentiated. From TG and IR data, elimination of water takes place in two stages in the 20–200 °C temperature range. In diphosphates of the Sm–Yb series (type II) the OH loss occurs at higher temperatures than in those of the La–Sm series (type I). The elimination of OH groups leads to the decomposition of diphosphates and to exothermic peaks in the DTA/TG curves. XRD patterns of samples heated above 900 °C exhibit peaks due to polyphosphates formed during decomposition of diphosphates.[10] However, the decomposition process of the diphosphates is not simple, and further investigation is needed to explore different possible routes.

The XRD powder study of the samples showed the existence of two types of diphosphates. In the first group, Ln = La–Sm, all peaks in the XRD patterns were indexed according to an orthorhombic symmetry (type I). In the second group, the patterns were indexed using a triclinic cell (type II). In type I, the unit cell volume is approximately four times that of type II. Measurements of the sample density in the two diphosphates $LaHP_2O_7{\cdot}3.5H_2O$ and $YbHP_2O_7{\cdot}3.5H_2O$ lead to $\rho = 2.82$, and 3.29 g cm^{-3} respectively, which suggests the presence of eight diphosphate groups ($Z = 8$) per unit cell in type I and two diphosphate groups ($Z = 2$) in type II. In the case of Sm, both structures can be obtained, depending on the reactant concentrations.

The rare-earth cation size is an important parameter controlling the structural features of phosphates (Table 1). In Fig. 5 the dependence of the unit cell parameters on the rare-earth ionic radii, taken from Jia,[19] is shown. All cell parameters increase slightly with rare-earth metal size. This is similar to the observations reported in other related series in which different lanthanide cations can be substituted for without strong structural modifications (lanthanide contraction effect[20]). However, the existence of two structure types for the phosphates indicates that the arrangement of diphosphate groups is possible in two different ways. From analysis of the unit cell parameters, it appears that the triclinic form (type II) is a truly different arrangement, and not simply a distortion of the more symmetric orthorhombic type I. This observation is supported by the strong variation of volume per formula unit obtained (7%) in the two samarium diphosphates analyzed (Fig. 6), indicating that the two structures are not so similar.

From NMR and IR data, the diphosphate character was confirmed.[21–23] The detection of vibration modes of POP groups at *ca.* 750 cm^{-1} in the IR spectra and the position of

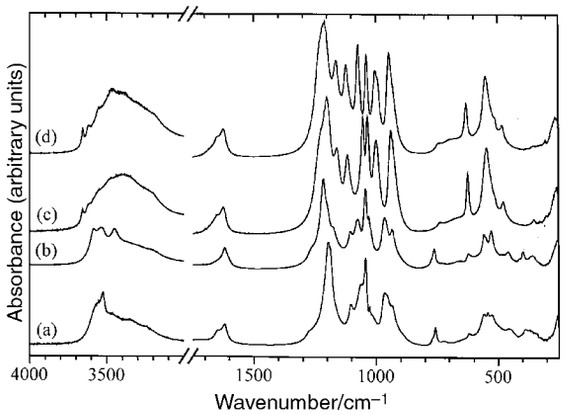

Fig. 3 IR spectra of $LaHP_2O_7{\cdot}3.5H_2O$ (a), $SmHP_2O_7{\cdot}3.5H_2O$ (type I) (b), $SmHP_2O_7{\cdot}3.5H_2O$ (type II) (c), and $YbHP_2O_7{\cdot}3.5H_2O$ (d) recorded on samples diluted in KBr pellets.

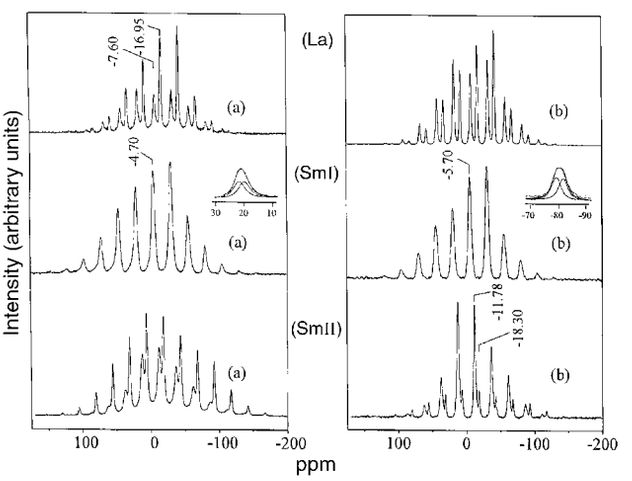

Fig. 4 ^{31}P MAS (a) and CP-MAS (b) NMR spectra of $LnHP_2O_7{\cdot}3.5H_2O$, with Ln = La and Sm. In the Sm diphosphate, the spectra correspond to the two identified structural types.

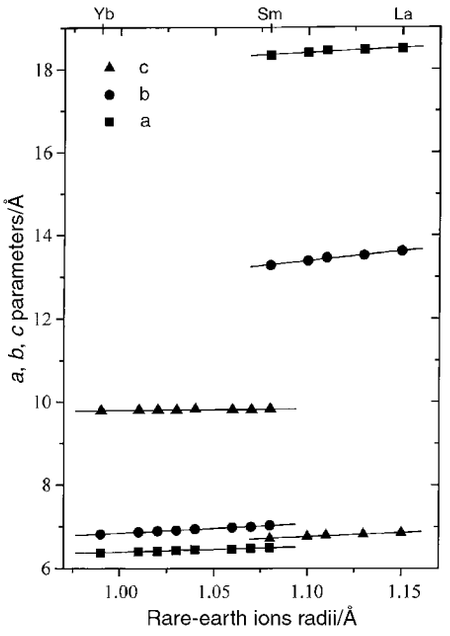

Fig. 5 Dependence of unit cell parameters on ionic radii for eight-fold lanthanide coordination.

NMR components at *ca.* −20 ppm confirms the existence of diphosphate groups in these compounds. From the positions of ν_a(POP) and ν_s(POP) vibrations in the IR spectra, POP groups are assumed to adopt a bent configuration,[24] since the existence of linear POP groups would lead to a more important separation of the two infrared POP bands. Finally, the presence of a band at 3200 cm^{-1}, that does not disappear when all water has been eliminated, confirms the existence of OH groups in these diphosphates.

Based on the lower antishielding effect on the NMR signal of OH with respect to OLn bonds, the NMR component located at more positive chemical shift values has been assigned to OH-bearing tetrahedral groups, (PO_3OH), and the second to PO_4 tetrahedra. These signals could not be resolved in the orthorhombic Sm diphosphate (type I). This assignment is confirmed by the CP-MAS technique, with which residual H–P dipolar interactions were eliminated preferentially from the first signal. The intensities of the two components are near 1 : 1 in the MAS spectra, suggesting that both signals probably correspond to the tetrahedra of the same diphosphate groups. From the variation in the intensities of the two components in the MAS and CP-MAS spectra, it was concluded that the disposition of protons with respect to the two tetrahedra is different in both structures. In the case of the diphosphates of

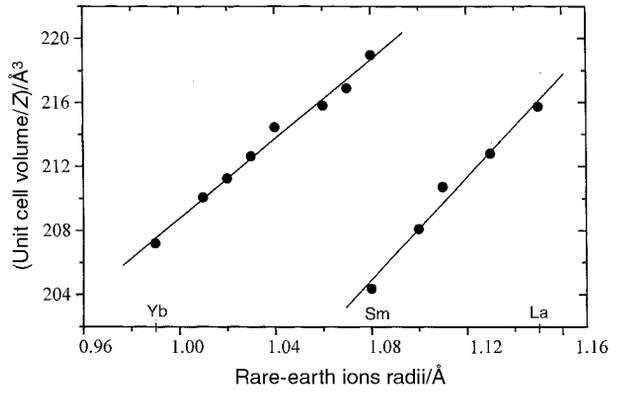

Fig. 6 Dependence of unit cell volume per formula unit on ionic radii for eight-fold lanthanide coordination.

type I [$LaHP_2O_7{\cdot}3.5H_2O$ and $SmHP_2O_7{\cdot}3.5H_2O$ (type II)] the relative intensity of the two components does not change indicating that the magnetization transfer from protons to the two P atoms is equivalent. However, in the diphosphates of type II [$SmHP_2O_7{\cdot}3.5H_2O$ (type II)] both P atoms receive the magnetization in a different way; in particular, the signal intensity of P atoms with OH groups is clearly higher than that of P atoms in PO_4 environments. It was concluded that hydrogen bonds established between contiguous tetrahedra (P–O–H–O–P) could be more symmetric in the first case, and asymmetric (P–O–H···O–P) in the second.

Conclusions

XRD, IR and NMR (MAS and CP-MAS) techniques have been used to characterize $HLnP_2O_7{\cdot}3.5H_2O$ compounds obtained from acidic mixtures of $Na_4P_2O_7$ and $LnCl_3$ solutions. DTA/TG curves showed the existence of water losses due to elimination of water of crystallization and OH groups.

The XRD analysis indicated the existence of two types of diphosphates. Indexing of the powder patterns of the first group, Ln = La–Sm, was done using an orthorhombic cell and those of the second group, Ln = Sm–Yb, using a triclinic one. The unit cell volume of the first group of diphospates is nearly four times larger than that of the second group. Moreover, the volume per formula unit decreases by 7% when going from the triclinic to orthorhombic samarium diphosphates. Differences in the symmetry of the two diphosphates were confirmed by IR spectroscopy.

From the IR data, a non-linear arrangement of P_2O_7 groups was deduced. Two structural environments for P atoms: PO_4 and PO_3OH, were identified by NMR. The variation of the intensities of two components in the MAS and CP-MAS experiments was interpreted by assuming that hydrogen bonds connecting neighboring diphosphate groups are different in both diphosphates. Structural confirmation of these points requires the analysis of single crystals.

References

1 H. P. Weber, T. C. Damen, H. G. Danielmeyer and B. C. Tofield, *Appl. Phys. Lett.*, 1973, **22**, 534.
2 S. R. Chinn and H. Y.-P. Hong, *Opt. Commun.*, 1975, **15**, 345.
3 K. Otsuka and T. Yamada, *Appl. Phys. Lett.*, 1975, **26**, 311.
4 M. Saruwatari, T. Kimura and K. Otsuka, *Appl. Phys. Lett.*, 1976, **29**, 291.
5 J. Nakano, K. Otsuka and T. Yamada, *Appl. Phys. Lett.*, 1976, **47**, 2749.
6 K. Otsuka, Y. Miyazawa and T. Yamada, *J. Appl. Phys.*, 1977, **48**, 2099.
7 M. Saruwatari, K. Otsuka, Y. Miyazawa, T. Yamada and T. Kimura, *J. Quantum Electron.*, 1977, **13**, 836.
8 J. E. Marion and M. J. Weber, *Eur. J. Solid State Inorg. Chem.*, 1991, **28**, 271.
9 K. Kubodera, Y. Miyazawa, J. Nakano and K. Otsuka, *Opt. Commun.*, 1978, **27**, 345.
10 M. Kizilyalli, *J. Less-Common Metals*, 1987, **127**, 147.
11 Y. V. Tananaev, V. G. Kuznetsov and V. P. Vasil'eva, *Inorg. Mater.*, 1967, **3**, 87.
12 E. G. Afonin and N. I. Pechurova, *Russ. J. Inorg. Chem.*, 1990, **35**, 783.
13 Bruker WINFIT Program, *Bruker Report*, 1994, **140**, 43.
14 P. E. Werner, L. Eriksson and M. Westdahl, *J. Appl. Crystallogr.*, 1985, **18**, 367.
15 P. M. Wolff, *J. Appl. Crystallogr.*, 1968, **1**, 108.
16 G. S. Smith and R. L. Snyder, *J. Appl. Crystallogr.*, 1979, **12**, 60.
17 A. Boultif and D. Louer, *J. Appl. Crystallogr.*, 1991, **24**, 987.
18 N. N. Chudinova, G. M. Balagina and L. P. Shklover, *Izv. Akad. Nauk SSSR, Neorg. Mater.*, 1977, **13**, 2075.
19 Y. Q. Jia, *J. Solid State Chem.*, 1991, **95**, 184.
20 N. Yu. Anisimova, N. N. Chudinova and V. K. Trunov, *Inorg. Mater.*, 1993, **291**, 94.
21 L. Griffiths, A. Root, R. K. Harris, K. J. Parker,

A. M. Chippendale and F. R. Tromans, *J. Chem. Soc., Dalton Trans.*, 1986, 2247.
22 A. Cheetham, N. J. Clayden, C. M. Dobson and R. J. B. Jakeman, *J. Chem. Soc., Chem. Commun.*, 1986, 194.
23 S. Prabhakar, K. J. Rao and C. N. R. Rao, *Chem. Phys. Lett.*, 1987, **139**, 96.
24 M. Harcharras, A. Ennaciri, A. Rulmont and B. Gilbert, *Spectrochim. Acta, Part A*, 1997, **53**, 345.